Role of the Bile Salt Surfactant Sodium Cholate in Enhancing the Aqueous Dispersion Stability of Single-Walled Carbon Nanotubes: A Molecular Dynamics Simulation Study

Shangchao Lin[†,‡] **and Daniel Blankschtein***[,†]

Departments of Chemical Engineering and Mechanical Engineering, Massachusetts Institute of Technology, Cambridge, Massachusetts 02139, United States

Received: August 12, 2010; Revised Manuscript Received: October 15, 2010

Very recently, bile salt biosurfactants have been utilized extensively to disperse individual single-walled carbon nanotubes (SWNTs) in aqueous solution with high weight fractions, as well as to sort SWNTs according to their electronic properties with the aid of ultracentrifugation. To help elucidate the role of bile salts in the SWNT dispersion process, we report the first detailed large-scale all-atomistic molecular dynamics (MD) simulation study of the adsorption and surface self-assembly of a common bile salt surfactant, sodium cholate (SC), on a SWNT in aqueous solution. We find that the cholate ions wrap around the SWNT like a ring and have a small tendency to orient perpendicular to the cylindrical axis of the SWNT, a unique feature that has not been observed for conventional linear surfactants such as sodium dodecyl sulfate (SDS). In addition, we carry out a series of simulations to compute the potential of mean force (PMF) between two parallel SC-covered SWNTs as a function of the intertube separation. By comparing our simulated PMF profile of SC with the PMF profile of SDS reported in the literature, we found that, at the saturated surface coverages, SC is a better stabilizer than SDS, a finding that is consistent with the widespread use of SC to disperse SWNTs in aqueous media. Indeed, the superior dispersion-induced stability of SC over SDS results from a higher repulsive energy barrier and a shallower attractive energy well induced by SC in the PMF profile. In particular, we found that the shallower attractive energy well induced by SC is due to the rigid, bean-like structure of SC which allows this bile salt surfactant to more effectively accommodate the intertube gap.

1. Introduction

Since the first successful use of surfactants to disperse carbon nanotubes, a highly water insoluble material, in aqueous solution,[1] surfactants have played a very important role in the standard procedure used to prepare aqueous dispersions of single-walled carbon nanotubes (SWNTs).[2−5] Specifically, this widely recognized, surfactant-aided dispersion process involves the application of an external energy input (ultrasound) to separate nanotubes at the bundled end by overcoming the strong van der Waals (vdW) attractions between them.[5,6] Subsequently, the separated bundled ends provide new adsorption sites for the surfactant molecules. As a result, the repulsive potential energy resulting from the adsorbed surfactant molecules (electrostatic for ionic surfactants and steric for nonionic surfactants) further enhances this separation process.[1,2,6] In the case of ionic surfactants, the electrostatic repulsion between the surfactant-covered SWNTs has been quantified experimentally by measuring the zeta potential of the surfactant−SWNT assembly using electrophorisis.[7] Eventually, in a so-called "unzippering" fashion, individually isolated surfactant-coated carbon nanotubes are released to the aqueous solution.[6] This process involving the noncovalent dispersion of SWNTs in aqueous solution is essential for many applications of carbon nanotubes, including their use as chemical and biological sensors in aqueous environments such as living cells.[8−10]

In recent years, significant effort has been devoted to (i) better understand the unzippering mechanism, and (ii) screen through many types of surfactants for the preparation of high-weight fraction, aqueous solutions of SWNTs, including ranking of surfactants in terms of their ability to solubilize unbundled SWNTs.[2,3,5,6,11−13] In order to obtain a high-quality SWNT aqueous solution for practical applications, surfactants are not only required to increase the weight fraction (or the solubility) of unbundled SWNTs but also to stabilize the individual nanotubes against rebundling, thus increasing the shelf life of these colloidal dispersions. In particular, the anionic surfactant SDS has been used extensively to separate SWNT bundles, as well as to stabilize individual nanotubes with the aid of ultrasonication.[1,5]

Very recently, more attention has been devoted to bile salts, the biological detergents, which have been shown to solubilize individual SWNTs in aqueous solution with high weight fractions.[13] In particular, the most common bile salt, sodium cholate (SC), has been utilized to both separate and sort SWNTs according to their different diameters and electronic properties with the aid of both ultrasonication and ultracentrifugation.[14,15] Bile salts, unlike conventional linear surfactants such as SDS, are rigid facial amphiphiles (referred to as "two-faced detergents"; see Figure 1 for the chemical structure of SC). These surfactants possess a quasiplanar, slightly bent but rigid steroid ring with a hydrophilic face (the hydroxyl groups and the charged carboxylate group) and a hydrophobic face (the methyl groups and the tetracyclic carbon backbone) residing back-to-back.[16] As a result of their unique chemical structure, bile salts act as very effective dispersants of biological molecules in living cells, including fat-soluble vitamins, bilirubin, and cholesterol.[17] Very recently, new dispersants have been synthesized based on the "two-faced" bile salt motif in order to stabilize cylindrically

* Corresponding author. Phone: (617) 253-4594. Fax: (617) 252-1651. E-mail: dblank@mit.edu.
† Department of Chemical Engineering.
‡ Department of Mechanical Engineering.

10.1021/jp1076406
Published on Web 11/04/2010

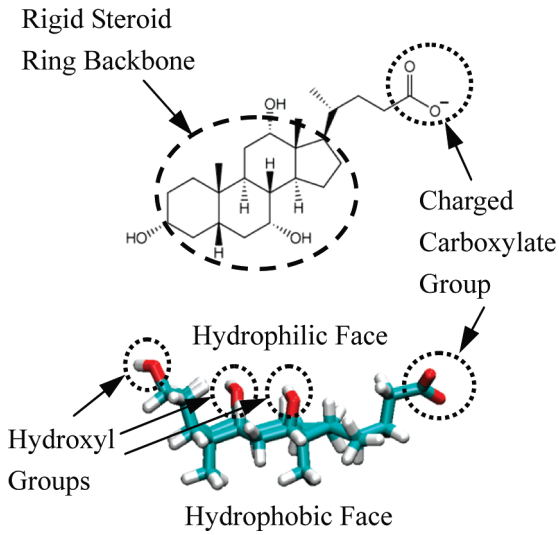

Figure 1. Schematic (top) and spatial (bottom) chemical structures of sodium cholate, a common bile salt surfactant, showing the rigid steroid-ring backbone, the hydrophobic and hydrophilic faces of the molecule, the hydroxyl groups (OH), and the charged carboxylate group (COO^-). Color code: red, oxygen; light green, carbon; white, hydrogen.

shaped integral membrane proteins.[18] Furthermore, it is believed that, due to the slightly bent but rigid steroid ring found in bile salts, these surfactants can very effectively accommodate the curvature of the SWNT surface and, as a result, can better enhance the dispersion stability of SWNTs in aqueous solutions.[13,14,19,20]

To date, molecular dynamics (MD) simulations of surfactant adsorption and surface self-assembly on SWNTs have focused primarily on conventional linear surfactants such as SDS,[21−23] as well as on single-tailed and double-tailed phosphatidylcholine,[24−26] using all-atomistic or course-grained force fields to model the surfactants and carbon nanotubes. Very recently, interactions between two SDS-coated SWNTs were studied using MD simulations, including elucidating the contributions from electrostatic and vdW interactions to the simulated potential of mean force (PMF) between the two SWNTs.[23] In addition, very recently, density differences of SC−SWNT assemblies when cholate ions adsorb onto SWNTs having different diameters have been studied using MD simulations.[27,28] However, the surface morphology of adsorbed SC as a function of its surface coverage have not been investigated computationally. Note that, experimentally, increasing the surfactant concentration beyond the surfactant critical micelle concentration (CMC) results in negligible increases in both surfactant surface coverage at interfaces and in surfactant monomer concentration. This follows because, in general, above the CMC, the added surfactant molecules increase primarily the micelle population.[29,30] In addition, in recent MD simulations of surfactant adsorption onto solid surfaces, no desorption of surfactant monomers from the solid surface was observed, which does not ensure thermodynamic equilibrium of the simulated system. Recall that in a thermodynamically equilibrated aqueous system, where water, surfactants, and SWNTs are present, surfactant molecules adsorbed onto the SWNTs should have the same chemical potential as the surfactant monomers desorbed from the SWNTs. Accordingly, the surfactant monomer concentration should be nonzero to avoid unphysical chemical potential values.[31] Moreover, the mechanism underlying the surfactant-induced stabilization of aqueous dispersions of SWNTs is not sufficiently well understood to permit a rational design of suitable surfactants.

With all of the above in mind, in the present study, we carried out a large-scale (up to 43 000 atoms), extended-time (up to 240 ns), and all-atomistic MD simulation to investigate the adsorption and surface self-assembly of SC, at low and high total SC concentrations, around a SWNT as a function of the resulting SC surface coverage. A limitation typical to all-atomistic MD simulations is that due to the currently available computational resources, it is impossible to simulate large enough systems to determine the adsorption isotherm of SC on SWNTs, including the resulting saturated SC surface coverage on the SWNTs. Note that under saturated SC surface coverage, SC surfactant micelles begin to form. Unfortunately, at dilute aqueous solution conditions where there are so many water molecules in the simulation box to accommodate surfactant monomers and micelles, the simulations become very costly computationally. Therefore, we carried out simulations at a sufficiently high total SC concentration to be able to reproduce the experimentally estimated saturated SC surface coverage on the SWNT.[19,32] Although on the basis of our discussion above, where we expect that not all the SC monomers will adsorb onto the SWNT surface, the simulated surface coverage should nevertheless be similar to the experimental value because of the small concentration of desorbed SC monomers (typically, less than the CMC of SC at around 16.3 mM[33]). In our simulations, SC monomers will coexist with adsorbed cholate ions present in the SC−SWNT assembly, which is required for the system to attain thermodynamic equilibrium. After comparing the simulated average SC surface coverage and average bulk SC concentration with the experimental values, we confirmed that our simulations at high total SC concentration reproduce reasonably well the experimental saturated SC surface coverage on the SWNTs.[19] Details about the experimental and simulated values are presented later. More importantly, in order to quantify the interactions between SWNTs coated with cholate ions, we carried out a potential of mean force (PMF) calculation for two parallel SWNTs, as a function of intertube separation (defined as the distance between the cylindrical axes of the two SWNTs), d, with each SWNT covered with cholate ions at a surface coverage comparable to the saturated surface coverage deduced from our previous simulation at high total SC concentration. Subsequently, we decomposed the computed PMF profile into contributions resulting from the two parallel bare SWNTs and from sodium cholate. Moreover, we rationalized the mechanism responsible for the repulsive potential energy barrier and the attractive potential energy well in the PMF profile, resulting from sodium cholate, in terms of the long-range electrostatic repulsion, the short-range vdW attraction, and the short-range steric repulsion.

2. Methods

2.1. Computational Model. Simulations of sodium cholate adsorption and the associated surface self-assembly on the SWNT surface in aqueous solution were carried out using the GROMACS 4.0 software package.[34] A (6,6) single-walled carbon nanotube (with a diameter of 0.81 nm and a length of 6.16 nm, as determined based on the centers of mass of the carbon atoms) was selected as a representative SWNT. The simulated SWNT is sufficiently long compared to the size of a cholate ion (approximately 1.5 nm × 0.8 nm × 0.6 nm), which allows observation of the adsorption pattern of the cholate ions on the SWNT surface. The SWNT was kept rigid throughout the simulations, with all the carbon atoms in the nanotube treated as uncharged Lennard−Jones (LJ) spheres using the LJ parameters reported by Tummala et al.[21,22,35] Water molecules were modeled using the standard SPC/E model,[36] with bond lengths

constrained using the SETTLE algorithm.[37] SC molecules, which were assumed to completely dissociate into cholate ions and sodium counterions in water, were modeled using the OPLS-AA force field.[38] Bond lengths in the cholate ion were constrained using the parallel version of the LINCS algorithm.[39,40] van der Waals (vdW) attractions and hard-core steric repulsions were treated with a cutoff distance of 0.9 nm, which falls within the typical range of cutoff values used in other publications.[21,23] The vdW attractions and the hard-core steric repulsions between different atoms were calculated from the LJ potential using the standard geometric averaging rule which is implemented in the OPLS-AA force field.[38] Long-range electrostatic interactions were treated using the particle mesh Ewald (PME) summation method.[41,42]

The equations of motion were integrated with a time step of 2 fs using the Verlet (Leap-Frog) algorithm.[43,44] All the simulations were conducted under the NPT ensemble (constant number of atoms, constant pressure of 1.0 bar, and constant temperature of 298.15 K) in order to best mimic the experimental conditions. The velocity-rescaled Berendsen thermostat was implemented to maintain a constant temperature in the simulated system.[45] The pressure was coupled to an isotropic Berendsen barostat.[46] Periodic boundary conditions were applied in all three directions. In practice, most of the synthesized SWNTs are uncapped (to a larger extent when they undergo ultrasonication),[13] and therefore, in order to allow small molecules such as water and sodium counterions to fill the nanotube, the length of the simulation box was chosen to be about 0.9 nm longer than the nanotube length (recall that the diameter of a water molecule is around 0.35 nm using the OPLA-AA force field). The trajectories, velocities, and forces corresponding to all the atoms in the system were saved every 10 000 steps (20 ps) to satisfy the ergodicity criterion for data analysis.[47]

2.2. Simulated System. To probe the adsorption and self-assembly of SC on the SWNT surface, a single (6,6) SWNT was confined at the center of the simulation box, with its cylindrical axis oriented along the *z*-direction. In order to quantify the effect of surfactant concentration on the adsorption morphology, we positioned different numbers of cholate ions (15 and 25) around the nanotube. Note that having 25 cholate ions on the 6.16 nm long (6,6) SWNT in our simulation matches the experimentally reported saturated SC surface coverage on a SWNT.[19] Different numbers of added cholate ions correspond to different total concentrations of cholate ions, with 15 added cholate ions corresponding to a low concentration of 75 mM and 25 added cholate ions corresponding to a high concentration of 125 mM. Subsequently, the simulation box was filled with water molecules. In order to maintain electroneutrality, an appropriate number of water molecules were replaced by sodium counterions resulting from the added cholate ions. Each system was equilibrated for 240 ns, and only the last 20 ns of simulation were used for data analysis. The simulation was confirmed to have reached equilibrium by monitoring the SASAs (solvent-accessible surface areas) of the cholate ions and the nanotube as a function of time (see Figure S1 in the Supporting Information). SASA was traced out by a probe sphere of radius 0.2 nm (corresponding to the location of the first hydration shell),[48] which was rolled around the cholate ions or the nanotube to identify their solvent (water in this case)-accessible regions.[49] Note that the region on the nanotube covered by cholate ions is not taken into account in the SASA calculation because water molecules in this region are excluded by the adsorbed cholate ions. As a result, we believe that the simulated SASA can nicely quantify the dynamics of adsorption and desorption of SC on the SWNT surface, similar to what takes place when surfactants self-assemble to form micelles.[50] The simulated system size, including the total numbers of SC and water molecules, the total number of atoms, the size of the simulation box, and the total simulation time, are summarized in Table S1 in the Supporting Information.

To investigate the interactions between two parallel SC-coated (6,6) SWNTs, we calculated the potential of mean force (PMF) by numerically integrating, in a trapezoidal manner, the forces exerted to separate the two nanotubes at various intertube separations.[23,51] This integration process begins from the largest intertube separation of 3.48 nm (where the simulated force applied to separate the two nanotubes approaches zero) and proceeds to the smallest intertube separation of 1.08 nm (where the force applied resulting from the hard-core steric repulsion between the two nanotubes overshoots). The force exerted at the center of mass of each SWNT should include contributions from all the flexible molecules in the system, including the adsorbed cholate ions, the sodium counterions, and the water molecules. Note that the initial configuration of the SC−SWNT assembly was obtained from the final configuration of the previous SC adsorption and self-assembly simulations corresponding to a SC surface coverage close to saturation (resulting from the 125 mM total SC concentration). In addition, note that in order to compare our results for SC with those for SDS where no SDS monomers were present,[23] the monomeric SC were removed to generate the initial configuration for the PMF calculation, assuming that their contribution to the PMF results are small. In order to carry out the PMF calculation for SC, we constructed a series of initial configurations in a manner similar to that in the work by Xu et al. for SDS.[23] The first configuration was generated by placing two parallel SC−SWNT assemblies at an intertube separation of 3.48 nm, and then filling the simulation box with sufficient water molecules and an appropriate number of sodium counterions to maintain electroneutrality. Following that, the system was further equilibrated for 20 ps under the NPT ensemble. The subsequent initial configurations were constructed from the preceding final equilibrium configuration as follows: for a pair of parallel SC−SWNT assemblies, only the two parallel bare SWNTs were translated as rigid entities toward each other in increments of 0.04 nm, and subsequently, the system was equilibrated for 20 ps. Note that translating only the bare SWNTs allowed the cholate ions to reorganize on the SWNT surfaces to avoid collisions when the two SWNTs are very close to each other. More specifically, the PMF profile was constructed by carrying out a total of 61 MD simulations with the intertube separation decreasing from 3.48 to 1.08 nm. After obtaining all the initial configurations, each system was equilibrated for 20 ns under the NPT ensemble. For the simulated systems at various intertube separations, only the last 5 ns, corresponding to the equilibrated systems, were used for data analysis, including the PMF calculations. The equilibration of each simulation run was verified by the convergence of the cumulative average force (averaged from time zero to time t) as a function of time t, as shown in Figure S2 in the Supporting Information. The errors in the simulated PMF profile were estimated based on the errors of the simulated forces using the block-averaging method, while accounting for the integration process.[52] In addition, in order to decompose the contributions to the total PMF profile resulting from the two parallel bare SWNTs to obtain the net contributions of SC, ΔPMF, to the total PMF profile (the contribution of water is negligible, as will be discussed later), the forces required to

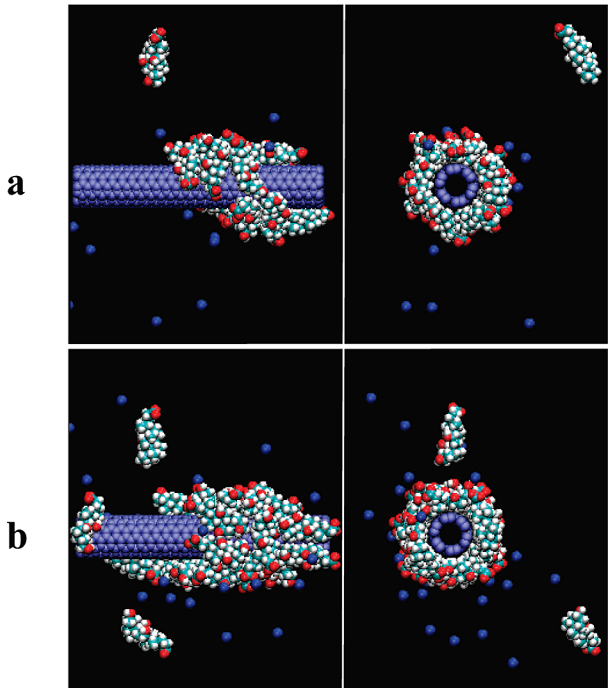

Figure 2. Representative postequilibrium simulation snapshots of a (6,6) SWNT in aqueous SC solutions at two different total SC concentrations: (a) 75 mM and (b) 125 mM. The two plots on the left are side views, and the two plots on the right are corresponding front views. Water molecules are not shown for clarity. Color code: red, oxygen; blue, sodium counterion; light green, carbon; white, hydrogen; purple, carbon atoms in the SWNT.

confine two parallel bare SWNTs at different intertube separations in vacuum were calculated in a similar manner using MD simulations, and the resulting PMF profile was calculated by integrating the forces.

3. Results and Discussion

3.1. Sodium Cholate Adsorption and Surface Self Assembly on a SWNT. Representative postequilibrium simulation snapshots of a (6,6) SWNT in aqueous SC solutions at total concentrations (that is, the total number of SC molecules divided by the volume of the simulation box) of 75 mM and 125 mM are shown in Figure 2. A common feature shared by both snapshots is that the cholate ions wrap around the SWNT like a ring with the hydrophobic faces pointing inward and the hydrophilic faces (having oxygen atoms shown as red spheres in Figure 2) pointing outward, as has been speculated in several recent experimental studies.[13,14,19,32] Note that the precise orientations of the cholate ions with respect to the cylindrical axis of the SWNT will be discussed later. Having the hydrophobic face pointing inward tends to maximize the contact between the hydrophobic faces of the cholate ions and the surface of the SWNT, as driven by the hydrophobic effect.[53] This organization of the cholate ions on the SWNT surface can be seen more clearly by comparing the radial distribution function (RDF) of the entire cholate ions (Figure 3a) relative to the RDF of the charged carboxylate groups (Figure 3b): the charged carboxylate groups (with the largest peak at around 1.2 nm at both 75 mM and 125 mM) are positioned farther away from the cylindrical axis of the SWNT than the entire cholate ions (with the largest peak at around 0.8 nm at both 75 mM and 125 mM).

Another interesting feature that can be seen in Figure 2 is that the adsorbed cholate ions prefer to distribute in a very

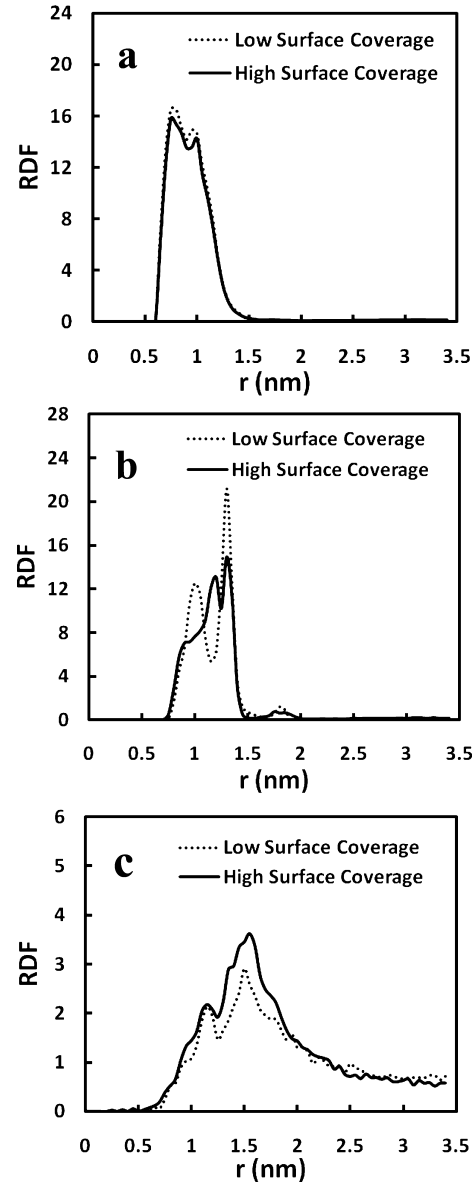

Figure 3. Simulated radial distribution functions (RDFs) relative to the cylindrical axis of a SWNT ("r" is measured radially from this axis): (a) RDF of the cholate ions, (b) RDF of the carbon atoms of the charged carboxylate groups, and (c) RDF of the sodium counterions. The RDFs are plotted for low (corresponding to a total SC concentration of 75 mM) and high (corresponding to a total SC concentration of 125 mM) SC surface coverages. Note that the radius of the (6,6) SWNT considered here is around 0.55 nm when excluded-volume effects are accounted for, and explains why the three RDF profiles shown remain zero for $r \leq 0.55$ nm.

compact manner around the SWNT, independent of their surface coverage on the SWNT surface. This is reflected in the RDF profiles in Figure 3a, where the shape of the RDF curves corresponding to the cholate ions is nearly independent of the total SC concentration. The RDF profiles in Figure 3a further indicate that this compact layer of cholate ions is located within 1.5 nm around the SWNT (since the two RDF curves decay to almost zero beyond 1.5 nm) and have a thickness of around 0.9 nm (as reflected in the width of the RDF curve in Figure 3a). This finding for SC is very different than for SDS, where the RDF becomes wider (the SDS molecules organize perpendicular to the SWNT surface) as the SDS surface coverage increases.[21,23] This unique surface adsorption morphology of SC, compared to those of more conventional surfactants possessing

TABLE 1: Population Analysis Results and Relevant Experimental Data

system	average number of adsorbed cholate ions	average number of monomeric cholate ions	average SC surface coverage (molecules/nm^2)	linear packing density of SC (molecules/nm)	average monomeric concentration of SC (mM)
1[a]	13.87	1.13	0.89	2.25	5.6
2[b]	21.84	3.16	1.39 (1.53 ± 0.34)[c]	3.55 (3.60 ± 0.80)[c]	15.6 (16.3)[d]

[a] Sodium cholate adsorption and surface self-assembly simulations on single (6,6) SWNTs under the low total SC concentration of 75 mM. [b] Sodium cholate adsorption and surface self-assembly simulations on single (6,6) SWNTs under the high total SC concentration of 125 mM. [c] The numbers in parentheses are the experimental values for the saturated surface coverage of cholate ions around a (6,5) SWNT from ref 19. [d] The number in parentheses is the experimental CMC of sodium cholate from ref 33.

flexible linear tails,[21−26] results from the rigid, steroid-ring structure of SC (see Figure 1).

Another common feature shared by the two side-view simulation snapshots in Figure 2 is that, instead of distributing uniformly around the nanotube,[13,19] the adsorbed cholate ions prefer to self-assemble side-by-side (see Figure S3a in the Supporting Information for zoomed-in snapshots), due to the hydrophobic effect.[53] Note that this side-by-side SC organization tends to minimize contact between the hydrophobic faces of the cholate ions and water, similar to what has been reported in the case of SDS adsorption onto SWNTs.[21] This side-by-side SC self-assembly is also facilitated by the condensation (or binding) of positively charged sodium counterions onto single, or multiple, negatively charged cholate ions (typically, onto the charged carboxylate groups, as shown in Figures S3b and S3c in the Supporting Information). Similar to what has been reported in the case of SDS adsorption onto SWNTs,[21,35] this sodium counterion condensation shields the electrostatic repulsions between the charged carboxylate groups and effectively brings them closer to each other. This interesting feature can also be seen in Figure 3c, where the largest peak of the RDF of the sodium counterions around the SWNT (at around 1.5 nm) is closely located to the largest peak of the charged carboxylate groups (at around 1.2 nm, see Figure 3b), reflecting the strong electrostatic attractions between these oppositely charged groups. The difference in the positions of these two peaks, 0.3 nm, reflects the center-to-center distance between a sodium counterion and a charged carboxylate group at contact.

As shown in Figure 2, as the total SC concentration increases from 75 mM in (a) to 125 mM in (b), both the number of cholate ions adsorbed on the SWNT surface and the number of cholate ions in the aqueous phase away from the SWNT increase. In particular, the monomeric SC concentration (that is, the number of SC monomers divided by the size of the simulation box) in Figure 2b is doubled compared to that in Figure 2a. In order to relate the SC surface coverage to the monomeric SC concentration, we carried out a population analysis at different total SC concentrations. On the basis of this population analysis, we found that different total SC concentrations yield different SC surface coverages and related monomeric SC concentrations. The time-averaged number of cholate ions adsorbed on the SWNT surface was computed by integrating the number density profiles (RDF times the average number density) of the cholate ions around the SWNT up to a cutoff distance of 1.5 nm, within which the cholate ions are considered to be adsorbed on the nanotube, and beyond which the cholate ions are considered as monomers. The computed average numbers of adsorbed cholate ions at 75 mM and 125 mM are consistent with the results based on a visual analysis of the postequilibrium simulation snapshots shown in Figure 2. Subsequently, the SC surface coverage was computed based on the diameter of 0.81 nm for the 6.16 nm long (6,6) SWNT that we simulated. In addition, estimating the average monomeric SC concentrations at different total SC concentrations is quite straightforward. Specifically, the average number of SC monomers is equal to the difference between the total number of SC molecules present in the simulation box and the average number of SC molecules adsorbed on the nanotube. Detailed results of the population analysis discussed above are reported in Table 1, where we have also reported experimental values of the saturated SC surface coverage on SWNTs[19] and of the CMC of SC[33] (a very good indicator of the monomeric SC concentration), in order to compare our population analysis results at 75 mM and 125 mM with experiment.

As shown in Figure 2a, at the low total SC concentration of 75 mM, the majority of the cholate ions adsorb onto the SWNT surface, which results in an average SC surface coverage of 0.89 molecule/nm^2 and an average monomeric SC concentration of 5.6 mM (see Table 1). As shown in Figure 2b, at the high total SC concentration of 125 mM, more cholate ions adsorb onto the SWNT surface, which results in an average surface coverage of 1.39 molecule/nm^2 and an average monomeric SC concentration of 15.6 mM (see Table 1). As expected, since we chose the high total SC concentration of 125 mM to reproduce the experimental saturated SC surface coverage, the simulated surface coverage at 125 mM (1.39 molecule/nm^2) agrees well with the experimental value of 1.53 ± 0.34 molecules/nm^2 estimated for a (6,5) SWNT (see Table 1).[19] It is interesting to recognize that, based on our simulations under the saturated SC surface coverage, cholate ions can only partially cover the SWNT surface, consistent with the experimentally estimated ratio of around 70%.[19] This should be contrasted with the SDS case, where dodecyl sulfate ions can completely cover the SWNT surface based on both experimental and simulation observations.[1,21,23] Note that the saturated SC surface coverage was estimated based on the linear packing density of 3.6 ± 0.8 cholate ions adsorbed per unit length (in nm) on (6,5) SWNTs (with a diameter of 0.75 nm, as calculated based on the centers of mass of the carbon atoms), which was estimated based on the density of SC−SWNT assemblies measured using an analytical ultracentrifuge in a 46 mM SC solution.[19] For our estimation, we have assumed that the linear packing density of SC on the experimentally studied (6,5) SWNTs is the same as that on the (6,6) SWNTs considered here due to the similar diameters of these two SWNTs. Although the total SC concentration studied in ref 19 (46 mM) is higher than the CMC of SC (16.3 mM),[33] in view of our previous discussion, the saturated SC surface coverage should be independent of the experimental total SC concentration beyond the CMC of SC. In addition, note that the estimated monomeric SC concentration of 15.6 mM at the simulated total SC concentration of 125 mM is similar to the experimental CMC of SC (16.3 mM[33]), confirming that the SC surface coverage on the SWNTs that we obtained at 125 mM reproduced reasonably well the experimental saturated SC surface coverage. Note that, due to the limited simulation box size, if the total SC concentration in the simulation box is further increased, the SC surface coverage on the SWNTs would continue to increase beyond the experi-

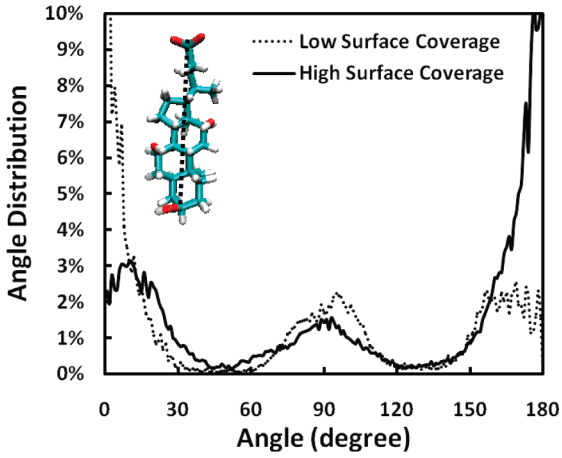

Figure 4. Simulated distribution profiles of the angle, θ, between the principal axis of the cholate ions and the cylindrical axis of the SWNT. Note that bias resulting from variations in solid angle has been removed by a weighting factor of (1/sin θ). In the SC molecular structure shown, the dotted line connecting the carbon atom in the carboxylate group with the carbon atom at the end of the steroid ring defines the principal axis of the cholate ion (refer also to Figure 1).

mental saturated SC surface coverage (more cholate ions would adsorb onto the SWNTs instead of contributing to an increase in the micelle population).[21,23−26,30] As a result, it is inappropriate to simulate even higher total SC concentrations. However, in future studies, coarse-grained models may be implemented based on our simulation results (e.g., the RDF profiles of the cholate ions, the charged carboxylate groups, and the sodium counterions around the SWNT) to more accurately calculate the adsorption isotherm of SC on SWNTs.

As discussed earlier, the cholate ions prefer to wrap around the SWNT like a ring. However, the precise orientations of the cholate ions with respect to the cylindrical axis of the SWNT still need to be determined. For this purpose, we calculated the distribution of the angles between the principal axis of the cholate ions (defined in Figure 4) and the cylindrical axis of the SWNT. As shown in Figure 4, for both SC surface coverages, the cholate ions prefer to orient almost parallel to the cylindrical axis of the SWNT (the largest peaks in the angle distribution profile are close to 0° and 180°), consistent with observations in recent MD simulations of SDS-coated SWNTs.[21,23] In addition, Figure 4 shows that the cholate ions also have a small tendency to orient perpendicular to the cylindrical axis of the SWNT (the angle distribution profile also exhibits a smaller peak at around 90°) to accommodate their own slightly bent planar chemical structures with respect to the curved SWNT surface, an interesting finding that is consistent with recent speculative experimental reports.[19,32] Note that the perpendicular orientation of the cholate ions can be clearly seen in Figure S3 a. This multipeak feature in the angle distribution profile may reflect the fact that adsorbed cholate ions need to adapt both configurations to accommodate the SWNT circumference. This is indeed driven by the need to form a closed ring consisting of a discrete number of cholate ions in order to wrap around the SWNT. This last finding suggests that the orientation of the cholate ions relative to the cylindrical axis of the SWNT may vary as a function of the nanotube diameter, due to the rigidity of the cholate ions, a unique feature which has not been observed with other conventional surfactants possessing flexible linear hydrocarbon chains.[21,23] In the future, it will be interesting to carry out MD simulations as a function of nanotube diameter to further corroborate this suggestion.

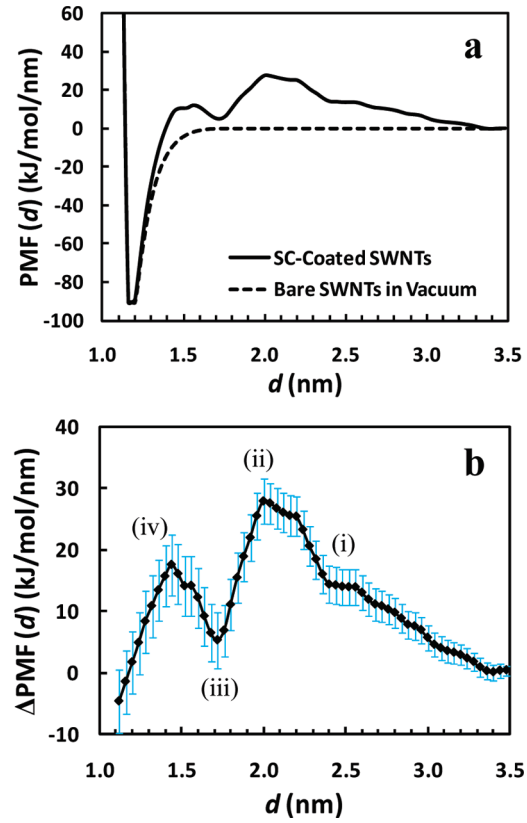

Figure 5. (a) Simulated potential of mean force (PMF) corresponding to (i) two parallel SWNTs coated with cholate ions (solid line), and (ii) two parallel bare SWNTs in vacuum (dashed line), as a function of the intertube separation, d. Note that the two PMF profiles overlap for $d \leq 1.2$ nm, (b) Net contribution of SC to the PMF profile, ΔPMF, corresponding to two parallel SWNTs coated with cholate ions. The error bars (in blue) were computed using the block averaging method discussed in the text. Note that the y-axis in (b) has been rescaled relative to that in panel a for clarity. In addition, the designations i−iv in panel b correspond to plots a−d in Figure 7, where 2D atom number density plots of the cholate ions and the sodium counterions are shown at selected intertube separations in order to help explain the features exhibited by the ΔPMF profile discussed in the text.

3.2. Interactions between Two Parallel SWNTs with Adsorbed Cholate Ions. The interactions between two parallel SWNTs with cholate ions adsorbed at approximately the saturated SC surface coverage were quantified using the potential of mean force (PMF) per unit length (in nm) of the nanotube, as a function of the intertube separation, d, as shown by the solid line in Figure 5a. The simulated PMF profile exhibits a primary, long-range repulsive potential energy barrier possessing a maximum of around 28 kJ per mole per nanometer of the simulated SWNTs, extending from 2.0 to 3.48 nm (reflected by the fact that the slope of the PMF curve here is negative). This primary potential energy barrier prevents the SWNTs from approaching each other under the vdW attractions between the two SWNTs and, as a result, prevents coagulation of the SWNT aqueous dispersion. The PMF profile in Figure 5a also exhibits a secondary, attractive potential energy region extending from 1.7 to 2.0 nm (reflected by the fact that the slope of the PMF curve here is positive). The depth of this attractive energy well is around −23 kJ/mol/nm, which counterbalances most of the repulsive energy barrier and, as a result, the PMF profile approaches a small minimum of 5 kJ/mol/nm at around 1.7 nm. As the intertube separation decreases further from 1.7 to 1.5 nm, the PMF profile goes up again, giving rise to a small repulsive energy barrier of around 10 kJ/mol/nm.

Although in their recent simulations of SDS adsorption onto SWNTs, Xu et al. did not study the PMF profile of two parallel SDS-coated SWNTs at intertube separations smaller than 1.5 nm,[23] we extended our simulations to include this separation region in the case of sodium cholate. As the intertube separation decreases from 1.5 to 1.2 nm, the PMF profile drops sharply (the primary attractive energy region) and reaches an minimum energy well of around −90 kJ/mol/nm, as determined by the strong vdW attraction between the two parallel bare SWNTs (see the dashed line in Figure 5a). This reflects the fact that the separated SWNTs will eventually rebundle as a result of this minimum energy well, and therefore surfactants can only stabilize SWNTs in aqueous solutions temporarily through the induced repulsive energy barrier. Finally, as the intertube separation decreases further below 1.2 nm, the PMF profile goes up sharply, as determined by the hard-core steric repulsion between the two parallel bare SWNTs (note that the solid line and the dashed line overlap in this region, as shown in Figure 5a).

All the features of the PMF profile discussed above for sodium cholate agree well qualitatively with recent computational studies of grafted polymers,[54] the adsorbed cationic surfactant, n-decyltrimethylammonium chloride (DTMAC),[55] and the adsorbed anionic surfactant, SDS,[23,51] on SWNTs using mean-field theory,[54] statistical mechanics,[55] and MD simulations,[23,51] respectively. Comparing our PMF results for SC with those of Xu et al. for SDS,[23] we have found, quantitatively, that SC is more effective than SDS at stabilizing aqueous dispersions of individual SWNTs, when the SWNTs are covered with the saturated amounts of each surfactant type. Specifically, (i) the simulated potential energy barrier induced by SC at 2.0 nm is 40% higher than that induced by SDS at 2.4 nm,[23] and (ii) the simulated attractive energy well induced by SC at 1.7 nm (see Figure 5a) is 50% smaller than that induced by SDS at the same intertube separation.[23] Note that a shallower attractive energy well can still enhance the dispersion stability based on the theory of slow colloid coagulation,[56] where the integration of the exponential of the PMF between two colloidal particles (two SC-coated SWNTs in the present case) along the interparticle distance is inversely proportional to the coagulation rate of these two colloidal particles.

To further understand the mechanism responsible for the superior dispersion stability induced by SC, it is instructive to decouple the contribution resulting from the two parallel bare SWNTs (including the vdW attraction and the hard-core steric repulsion) to the total PMF profile. To this end, we subtracted the PMF profiles corresponding to the solid line (with SC) and the dashed line (without SC) in Figure 5a. The resulting net SC contribution, ΔPMF, to the total PMF profile is shown in Figure 5b, where we have assumed that the contribution due to the water molecules is negligible compared to that due to SC based on the recent studies by Xu et al. in the case of SDS.[23] This approximation may also be rationalized by the fact that the magnitude of the simulated PMF induced by water molecules is quite small when two SWNTs are present in pure water.[57] Note that, in general, water molecules only contribute to the repulsive energy barrier in the simulated PMF profile at small intertube separations ($d < 2.0$ nm considered here), when they are confined by the surfactant-coated SWNTs.[57] As a result, in the case of SC, this confinement-induced water repulsion is expected to slightly reduce the net contribution of SC to the simulated PMF profile at small intertube separations, while this water-induced repulsive contribution should be negligible at large intertube separations. The net contribution of SC to the PMF profile (the solid line in Figure 5b) exhibits features which are similar to those exhibited by the total PMF profile (the solid line in Figure 5a). This is due to the fact that the interaction between the two parallel bare SWNTs is negligible until the intertube separation decreases below 1.7 nm (see the dashed line in Figure 5a).

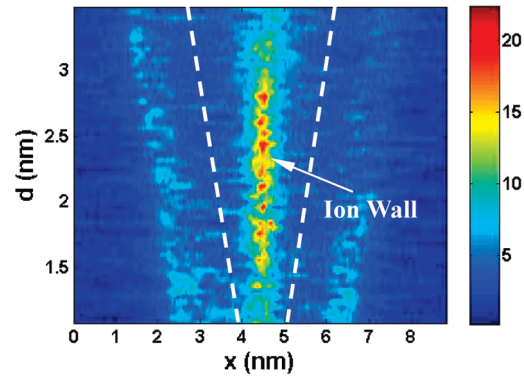

Figure 6. Simulated contour plot of the density profile of the sodium counterions (in units of kg/m^3) along the x-axis of the simulation box (which is parallel to d), as a function of the intertube separation, d. The density scale is shown in the side color bar. As shown, the ion wall extends from an intertube separation of $d = 1.7$ to $d = 2.8$ nm. The locations of the two SWNT cylindrical axes along the x-axis are shown by the two white dashed lines.

At intertube separations greater than 2.0 nm (see Figure 5b), the onset of the repulsive potential energy barrier in the ΔPMF profile is dominated by the long-range electrostatic repulsion between the two parallel SC-coated SWNTs, which behave as two parallel, negatively charged cylinders, mediated by the positively charged sodium counterions. This contribution to the potential energy barrier has been widely recognized as reflecting the electrostatic contribution which appears in the continuum DLVO theory.[7,29,58,59] Based on the Poisson−Boltzmann equation,[60] the electrostatic portion of the DLVO potential between two SC-coated SWNTs considered here is approximately proportional to the effective surface charge density on the SWNT surface, σ. Although the saturated surface coverage of SDS used in the recent MD simulations by Xu et al.,[23] as well as observed experimentally (2.8 molecules/nm^2),[61] is twice that of SC used in our MD simulations (1.4 molecule/nm^2),[19] after accounting for the effect of sodium counterion binding, the difference between the effective surface charge densities in the SC and the SDS cases should be greatly reduced. This expectation is consistent with the fact that the extent of sodium counterion dissociation for a SDS aggregate (= 0.124) is much smaller than that for a SC aggregate (= 1.000).[62] Our simulated number of sodium counterions bound to the charged carboxylate groups in cholate ions (under high total SC concentration) is consistent with the experimental observation of a high degree of sodium counterion dissociation associated with a SC aggregate (see Figure S4 in the Supporting Information for more details).

In addition to the repulsive electrostatic interaction described by the DLVO theory, other repulsive interactions operate between two SC-coated SWNTs.[29] In particular, the ion-induced steric repulsion[29,63,64] has been reported recently to play a role in repelling two SDS-coated SWNTs in the simulation study by Xu et al.[23] In fact, the existence of a concentrated ion wall can be seen in the simulated contour plot of the density profile of the sodium counterions along the x-axis of the simulation box (which is parallel to d), as a function of the intertube separation, d, as shown in Figure 6. The ion wall is defined

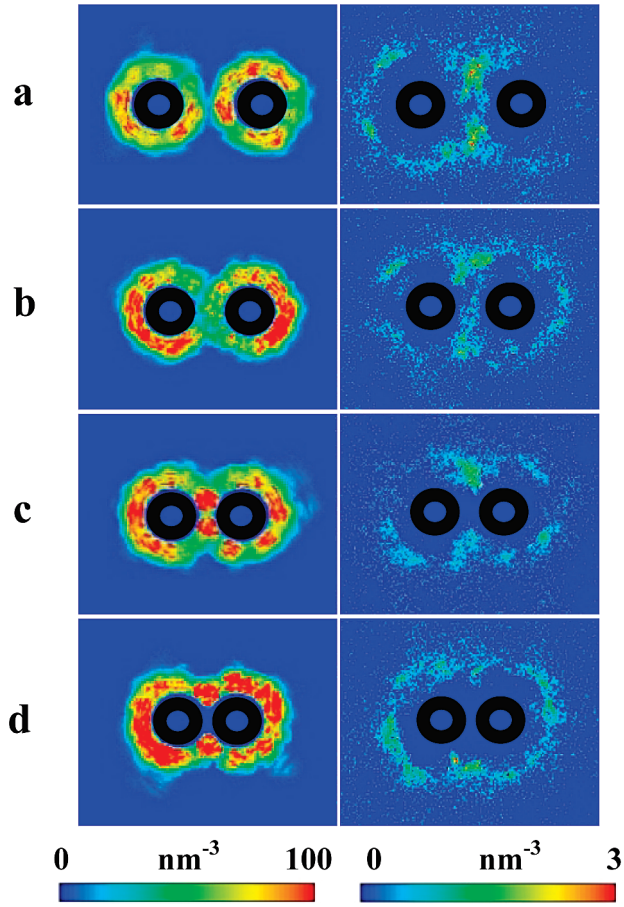

Figure 7. 2D atom number density plots of the cholate ions (left panel) and the sodium counterions (right panel) at selected intertube separations of (a) 2.48 nm, (b) 2.00 nm, (c) 1.68 nm, and (d) 1.32 nm. These four intertube separations were selected in order to help explain the features exhibited by the PMF profile discussed in the text. The atom number density scale is shown in the bottom color bars. The density plots in a−d represent front views of the simulation box. The black rings denote the locations of the two parallel SWNTs.

here as a layer of sodium counterions with a concentration of around 15 kg/m^3, which is two times greater than their bulk concentration of around 5 kg/m^3, following the same definition by Xu et al.[23] The ion wall is present at d values ranging from 1.7 to 2.8 nm (denoted by the red color in Figure 6). The existence of this ion wall can also be seen in the 2D atom number density plots (averaged along the cylindrical axis of the SWNT) of the sodium counterions at two intertube separations, as shown in Figure 7a and 7b. The fact that the ion wall in the case of SC spans a wider range of intertube separations (1.1 nm) than that in the case of SDS (0.9 nm)[23] may explain the higher potential energy barrier induced by SC. Indeed, if the ion-induced steric repulsive force in the SC case operates over a wider range of intertube separations, then, the potential energy barrier obtained by integrating the repulsive forces over this wider range of separations will be higher.

At shorter intertube separations below 2.0 nm (see Figure 5b), the cholate ions on the two SWNT surfaces begin to contact each other (the two green rings overlap in Figure 7b), which triggers direct interactions between them. These interactions between the cholate ions on the two SWNT surfaces results in the oscillatory behavior of the ΔPMF profile (for d values ranging from 1.08 to 2.0 nm in Figure 5b), which has been widely recognized to result from the interplay between the short-range vdW attraction and the short-range hard-core steric repulsion between molecules (the cholate ions in the present case) in close contact.[65] Note that once the two layers of cholate ions interleave with each other to merge into a single layer, the electrostatic force acting along the x-axis responsible for repelling the two parallel SWNTs will no longer exist. This oscillatory behavior, reflecting the molecularity of all condensed phases in nature, has been extensively studied experimentally in the case of liquids confined to molecular separations by two approaching smooth mica surfaces.[66−68] As expected, the continuum DLVO theory breaks down at molecular separations and fails to reproduce the oscillatory ΔPMF profile computed using MD simulations.

The interactions between cholate ions are shown in the 2D atom number density plots of the cholate ions at selected intertube separations to help explain the features exhibited by the ΔPMF profile (see Figure 7). Note that although the cholate ions on the SWNT surfaces begin to contact each other at a larger intertube separation of 2.48 nm (the two green rings begin to overlap in Figure 7a), the partially covered SWNT surface allows the cholate ions to exchange between the two nanotubes to efficiently cover the empty surface without incurring steric penalties (no red color within the intertube gap in Figure 7b). As expected, if the density of the cholate ions within the intertube gap is large (denoted by the red color in Figure 7c), then the cholate ions are confined and do exert a strong steric repulsive force between the two SWNTs. On the other hand, if the density of cholate ions within the intertube gap is small (denoted by the green color in Figure 7a and 7b), then the cholate ions have vacancies around them that can be filled and do exert a strong vdW attractive force between the two SWNTs. Therefore, the simulated oscillatory ΔPMF profile as the intertube separation decreases can be rationalized as follows: (i) the intertube gap begins to accommodate only a single layer of cholate ions from d = 2.0 to 1.7 nm (see Figure 7b), (ii) the two SWNTs begin to compress the single layer of cholate ions from d = 1.7 to 1.5 nm (see Figure 7c), and (iii) the single layer of cholate ions is squeezed out of the intertube gap, leaving a vacancy from d = 1.5 to 1.08 nm (see Figure 7d). Note that this relationship between the density of the cholate ions and the direction of the exerted force is analogous to the relationship between the density of cholate ions and the osmotic pressure within the intertube gap.[29] Note also that the mechanism underlying the vdW attraction between rigid molecules is slightly different from the bridging attraction between flexible polymers grafted onto colloidal particles,[29] contrary to the recent discussion in ref 23. Interestingly, when there is a single layer of sparsely packed cholate ions located within the intertube gap from d = 1.7 to 2.0 nm, the cholate ions are able to rotate (see Figure S5 in the Supporting Information) in order to fill the vacancy within this fixed intertube gap, due to their bean-like chemical structure. This unique feature of SC was not observed in the case of SDS, because of the linear, rod-like shape of the SDS molecule. As a result, the attractive energy well at d = 1.7 nm induced by sodium cholate is not as deep as that induced by SDS.

4. Conclusions

In summary, we report the first detailed large-scale all-atomistic MD simulation study of the adsorption and surface self-assembly of the bile salt surfactant, sodium cholate, on a (6,6) SWNT in aqueous solution. Our results on (i) the radial distribution function of the cholate ions around the cylindrical axis of the SWNT, and (ii) the distribution of the principal angles of the cholate ions with respect to the cylindrical axis of the

SWNT allow verification of previous speculations, featuring the "two-faced", slightly bent, rigid steroid-ring structure of bile salts. In addition, we studied the relation between the surface coverage of the cholate ions on the SWNT surface and the monomeric SC concentration by considering low and high total SC concentrations. We selected a high total SC concentration to carry out the simulations, so that the simulated surface coverage of the cholate ions would match the experimental SC saturated surface coverage. Subsequently, we utilized the final configuration of a single SC-coated SWNT, under this saturated surface coverage, to carry out a series of simulations to compute the PMF between two parallel SC-coated SWNTs as a function of intertube separation. The net contribution of sodium cholate to the PMF profile, ΔPMF, may be explained reasonably well by (i) the long-range electrostatic repulsion between the two SC-coated SWNTs (as described in the continuum DLVO theory) at large intertube separation, (ii) the short-range ion-induced steric repulsion at large intertube separation, and (iii) the short-range vdW attraction and steric repulsion (oscillatory force) induced by the adsorbed cholate ions at small intertube separation. By comparing our simulated PMF profile of SC with the PMF profile of SDS when the SWNTs are coated with the saturated surface coverages corresponding to each surfactant type, we are able to show that SC is a better stabilizer than SDS (it has a higher repulsive energy barrier and a shallower attractive energy well), a finding that is consistent with the widespread use of SC to disperse SWNTs in aqueous solution. In particular, the shallower attractive energy well induced by SC compared to that induced by SDS is due to the rigid, bean-like chemical structure of SC which allows this bile salt surfactant to more effectively accommodate the intertube gap.

We believe that the simulation study presented here enhances our quantitative and qualitative understanding of the role of bile salts such as SC in enhancing the dispersion stability of individual SWNTs in aqueous solution. Moreover, this study may shed light on the future design of novel surfactants capable of more efficiently stabilizing aqueous dispersions of nanoscaled materials. In the case of bile-salt analogues, such a design may include enhancing the hydrophilic face of the "two-faced" surfactants by attaching more hydrophilic groups on the carbon backbone, or modifying the rigid chemical structure of the "two-faced" surfactants to better accommodate the curvature of SWNTs.

Acknowledgment. This research was supported by funding provided by DuPont through the DuPont-MIT Alliance. Computational resources were partially supported by the Atlantic Computational Excellence Network (ACEnet) in Canada. The authors acknowledge helpful discussions with Professor Pak Yuet, Professor Michael Strano, Chih-Jen Shih, and Jonathan Mendenhall.

Supporting Information Available: Figures of (i) solvent-accessible surface areas (SASAs) of a SWNT and the cholate ions as a function of time (Figure S1), (ii) cumulative average forces applied on the two parallel SWNTs (Figure S2), (iii) zoomed-in plots of postequilibrium simulation snapshots of a SWNT in aqueous SC solutions (Figure S3), (iv) sodium counterion radial distribution function and number of sodium counterions around the charged carboxylate groups in cholate ions (Figure S4), and (v) postequilibrium simulation snapshots illustrating the orientation of one cholate ion within the intertube gap (Figure S5). A table summarizing the simulated systems (Table S1). This material is available free of charge via the Internet at http://pubs.acs.org.

References and Notes

(1) O'Connell, M. J.; Bachilo, S. M.; Huffman, C. B.; Moore, V. C.; Strano, M. S.; Haroz, E. H.; Rialon, K. L.; Boul, P. J.; Noon, W. H.; Kittrell, C.; Ma, J. P.; Hauge, R. H.; Weisman, R. B.; Smalley, R. E. *Science* **2002**, *297*, 593.

(2) Islam, M. F.; Rojas, E.; Bergey, D. M.; Johnson, A. T.; Yodh, A. G. *Nano Lett.* **2003**, *3*, 269.

(3) Moore, V. C.; Strano, M. S.; Haroz, E. H.; Hauge, R. H.; Smalley, R. E.; Schmidt, J.; Talmon, Y. *Nano Lett.* **2003**, *3*, 1379.

(4) Richard, C.; Balavoine, F.; Schultz, P.; Ebbesen, T. W.; Mioskowski, C. *Science* **2003**, *300*, 775.

(5) Vaisman, L.; Marom, G.; Wagner, H. D. *Adv. Funct. Mater.* **2006**, *16*, 357.

(6) Strano, M. S.; Moore, V. C.; Miller, M. K.; Allen, M. J.; Haroz, E. H.; Kittrell, C.; Hauge, R. H.; Smalley, R. E. *J. Nanosci. Nanotechnol.* **2003**, *3*, 81.

(7) Coleman, J. N. *Adv. Funct. Mater.* **2009**, *19*, 3680.

(8) Kong, J.; Franklin, N. R.; Zhou, C. W.; Chapline, M. G.; Peng, S.; Cho, K. J.; Dai, H. J. *Science* **2000**, *287*, 622.

(9) Kim, J. H.; Heller, D. A.; Jin, H.; Barone, P. W.; Song, C.; Zhang, J.; Trudel, L. J.; Wogan, G. N.; Tannenbaum, S. R.; Strano, M. S. *Nature Chem.* **2009**, *1*, 473.

(10) Lee, C. Y.; Sharma, R.; Radadia, A. D.; Masel, R. I.; Strano, M. S. *Angew. Chem., Int. Ed.* **2008**, *47*, 5018.

(11) Wang, H. *Curr. Opin. Colloid Interface Sci.* **2009**, *14*, 364.

(12) Matarredona, O.; Rhoads, H.; Li, Z. R.; Harwell, J. H.; Balzano, L.; Resasco, D. E. *J. Phys. Chem. B* **2003**, *107*, 13357.

(13) Wenseleers, W.; Vlasov, I. I.; Goovaerts, E.; Obraztsova, E. D.; Lobach, A. S.; Bouwen, A. *Adv. Funct. Mater.* **2004**, *14*, 1105.

(14) Arnold, M. S.; Green, A. A.; Hulvat, J. F.; Stupp, S. I.; Hersam, M. C. *Nature Nanotechnol.* **2006**, *1*, 60.

(15) Hersam, M. C. *Nature Nanotechnol.* **2008**, *3*, 387.

(16) Partay, L. B.; Jedlovszky, P.; Sega, M. *J. Phys. Chem. B* **2007**, *111*, 9886.

(17) Partay, L. B.; Sega, M.; Jedlovszky, P. *Langmuir* **2008**, *24*, 10729.

(18) Zhang, Q. H.; Ma, X. Q.; Ward, A.; Hong, W. X.; Jaakola, V. P.; Stevens, R. C.; Finn, M. G.; Chang, G. *Angew. Chem., Int. Ed.* **2007**, *46*, 7023.

(19) Arnold, M. S.; Suntivich, J.; Stupp, S. I.; Hersam, M. C. *ACS Nano* **2008**, *2*, 2291.

(20) Usrey, M. L.; Lippmann, E. S.; Strano, M. S. *J. Am. Chem. Soc.* **2005**, *127*, 16129.

(21) Tummala, N. R.; Striolo, A. *ACS Nano* **2009**, *3*, 595.

(22) Tummala, N. R.; Striolo, A. *Phys. Rev. E* **2009**, *80*, 021408.

(23) Xu, Z. J.; Yang, X. N.; Yang, Z. *Nano Lett.* **2010**, *10*, 985.

(24) Qiao, R.; Ke, P. C. *J. Am. Chem. Soc.* **2006**, *128*, 13656.

(25) Wallace, E. J.; Sansom, M. S. P. *Nano Lett.* **2007**, *7*, 1923.

(26) Wallace, E. J.; Sansom, M. S. P. *Nanotechnology* **2009**, *20*, 045101.

(27) Carvalho, E. J. F.; dos Santos, M. C. *ACS Nano* **2010**, *4*, 765.

(28) Quintilla, A.; Hennrich, F.; Lebedkin, S.; Kappes, M. M.; Wenzel, W. *Phys. Chem. Chem. Phys.* **2010**, *12*, 902.

(29) Israelachvili, J. N. *Intermolecular and surface forces: with applications to colloidal and biological systems*; Academic Press: London, 1985.

(30) Hiemenz, P. C.; Rajagopalan, R. *Principles of colloid and surface chemistry*, 3rd ed.; Marcel Dekker: New York, 1997.

(31) Smith, J. M.; Van Ness, H. C.; Abbott, M. M. *Introduction to chemical engineering thermodynamics*, 7th ed.; McGraw-Hill: Boston, 2005.

(32) Nair, N.; Kim, W. J.; Braatz, R. D.; Strano, M. S. *Langmuir* **2008**, *24*, 1790.

(33) Zhang, X. C.; Jackson, J. K.; Burt, H. M. *J. Biochem. Biophys. Methods* **1996**, *31*, 145.

(34) Hess, B.; Kutzner, C.; van der Spoel, D.; Lindahl, E. *J. Chem. Theory Comput.* **2008**, *4*, 435.

(35) Tummala, N. R.; Striolo, A. *J. Phys. Chem. B* **2008**, *112*, 1987.

(36) Berendsen, H. J. C.; Grigera, J. R.; Straatsma, T. P. *J. Phys. Chem.* **1987**, *91*, 6269.

(37) Miyamoto, S.; Kollman, P. A. *J. Comput. Chem.* **1992**, *13*, 952.

(38) Jorgensen, W. L.; Maxwell, D. S.; Tirado-Rives, J. *J. Am. Chem. Soc.* **1996**, *118*, 11225.

(39) Hess, B.; Bekker, H.; Berendsen, H. J. C.; Fraaije, J. G. E. M. *J. Comput. Chem.* **1997**, *18*, 1463.

(40) Hess, B. *J. Chem. Theory Comput.* **2008**, *4*, 116.

(41) Darden, T.; York, D.; Pedersen, L. *J. Chem. Phys.* **1993**, *98*, 10089.

(42) Essmann, U.; Perera, L.; Berkowitz, M. L.; Darden, T.; Lee, H.; Pedersen, L. G. *J. Chem. Phys.* **1995**, *103*, 8577.

(43) Hockney, R. W.; Goel, S. P.; Eastwood, J. W. *J. Comput. Phys.* **1974**, *14*, 148.

(44) Verlet, L. *Phys. Rev.* **1967**, *159*, 98.

(45) Bussi, G.; Donadio, D.; Parrinello, M. *J. Chem. Phys.* **2007**, *126*, 014101.

(46) Berendsen, H. J. C.; Postma, J. P. M.; Vangunsteren, W. F.; Dinola, A.; Haak, J. R. *J. Chem. Phys.* **1984**, *81*, 3684.
(47) Leach, A. R. *Molecular modelling: principles and applications*, 2nd ed.; Prentice Hall: Harlow, England, 2001.
(48) Stephenson, B. C.; Goldsipe, A.; Beers, K. J.; Blankschtein, D. *J. Phys. Chem. B* **2007**, *111*, 1025.
(49) Eisenhaber, F.; Lijnzaad, P.; Argos, P.; Sander, C.; Scharf, M. *J. Comput. Chem.* **1995**, *16*, 273.
(50) Stephenson, B. C.; Goldsipe, A.; Beers, K. J.; Blankschtein, D. *J. Phys. Chem. B* **2007**, *111*, 1045.
(51) Uddin, N. M.; Capaldi, F.; Farouk, B. *J. Eng. Mater. Technol.* **2010**, *132*, 021012.
(52) Flyvbjerg, H.; Petersen, H. G. *J. Chem. Phys.* **1989**, *91*, 461.
(53) Tanford, C. *The hydrophobic effect: formation of micelles and biological membranes*, 2nd ed.; Krieger: Malabar, FL, 1991.
(54) Shvartzman-Cohen, R.; Nativ-Roth, E.; Baskaran, E.; Levi-Kalisman, Y.; Szleifer, I.; Yerushalmi-Rozen, R. *J. Am. Chem. Soc.* **2004**, *126*, 14850.
(55) Patel, N.; Egorov, S. A. *J. Am. Chem. Soc.* **2005**, *127*, 14124.
(56) Fuchs, N. *Z. Phys. Chem., Abt. A:* **1934**, *171*, 199.
(57) Li, L. W.; Bedrov, D.; Smith, G. D. *J. Phys. Chem. B* **2006**, *110*, 10509.
(58) Booth, F. *J. Chem. Phys.* **1951**, *19*, 821.
(59) Chapot, D.; Bocquet, L.; Trizac, E. *J. Colloid Interface Sci.* **2005**, *285*, 609.
(60) As discussed in ref 29. The electrostatic repulsion of two charged parallel plates that are limited to small separations can be approximated as $U_{elec} \propto \alpha \ln(d)$ based on the Poisson−Boltzmann equation, where σ is the effective surface charge density of the plates. In the case of surfactant-covered SWNTs, we have assumed that this approximation also holds.
(61) Grossiord, N.; van der Schoot, P.; Meuldijk, J.; Koning, C. E. *Langmuir* **2007**, *23*, 3646.
(62) Bandyopadhyay, A.; Moulik, S. P. *Colloid Polym. Sci.* **1988**, *266*, 455.
(63) Khair, A. S.; Squires, T. M. *J. Fluid Mech.* **2009**, *640*, 343.
(64) Hui, Z. *J. Phys. Chem. C* **2010**, *114*, 8389.
(65) Israelachvili, J. N. *Philos. Mag. A* **1981**, *43*, 753.
(66) Horn, R. G.; Israelachvili, J. N. *J. Chem. Phys.* **1981**, *75*, 1400.
(67) Israelachvili, J. N.; Tandon, R. K.; White, L. R. *J. Colloid Interface Sci.* **1980**, *78*, 430.
(68) Pashley, R. M.; Israelachvili, J. N. *Colloids Surf.* **1981**, *2*, 169.

JP1076406